Analytically-derived Aerodynamic Force and Moment Coefficients of Resident Space Objects in Free-Molecular Flow

Kenneth A. Hart,[*] Soumyo Dutta,[†] Kyle R. Simonis,[‡]
Bradley A. Steinfeldt,[§] and Robert D. Braun[¶]

Georgia Institute of Technology, Atlanta, GA, 30332-1510, USA

Fast, high-fidelity trajectory propagation of objects in near-Earth orbits is a key capability for space situational awareness and mitigating probability of collisions on orbit. This high-fidelity analysis requires accurate aerodynamics prediction for objects in the free-molecular regime of flight, but most tools for aerodynamic prediction for this regime either are found using assumptions or are computationally intensive. Symbolic manipulation software can be used to analytically integrate expressions for pressure and shear pressure coefficients acting on a general body in free-molecular regime to derive aerodynamic force and moment expressions. The analytical aerodynamics prediction method is described and relations have been developed for the sphere, cylinder, panel, and rectangular prism. The NASA-developed Direct Simulation Monte Carlo Analysis Code is used to validate the analytical expressions and it is shown that expressions are accurate within 0.38%. These generalized analytic expressions in terms of angle of attack, sideslip angle, freestream conditions, wall temperature, and accommodation coefficients allow near-instantaneous computation of the rarefied aerodynamics and enables space situation awareness analysis.

Nomenclature

A	Area, m^2
C	Coefficient (see subscripts)
erf	Error function
$\mathbf{f}$	Force, N
H	Heaviside function
Kn	Knudsen number
l	Length, m
$\mathbf{n}$	Normal vector
p	Pressure, Pa.
R	Gas specific constant, J/kg-K
$\mathbf{r}$	Position vector
S	Region of integration
s	Molecular speed ratio
T	Temperature, K (see subscripts)
$\mathbf{t}$	Tangential vector
u	Surface parametrization variable
V	Velocity, m/s (see subscripts)
v	Surface parametrization variable
α	Angle of attack, rad

---

[*]Graduate Research Assistant, Daniel Guggenheim School of Aerospace Engineering, AIAA Student Member.

[†]Graduate Research Assistant, Daniel Guggenheim School of Aerospace Engineering, AIAA Student Member.

[‡]Undergraduate Research Assistant, Daniel Guggenheim School of Aerospace Engineering, AIAA Student Member.

[§]Research Engineer II, Daniel Guggenheim School of Aerospace Engineering, AIAA Member.

[¶]David & Andrew Lewis Professor of Space Technology, Daniel Guggenheim School of Aerospace Engineering, AIAA Fellow.

American Institute of Aeronautics and Astronautics

β	Sideslip angle, rad
λ	Mean free path, m
θ	Flow angle, rad
σ	Momentum accommodation coefficient (see subscripts)
τ	Shear force, Pa.

Subscript

A	Axial force
D	Drag force
i	Incident condition
l	Rolling moment
m	Pitching moment
N	Normal force
n	Yawing moment
p	Pressure
r	Reflected condition
ref	Reference quantity
S	Side force
T	Tangential force
w	Wall condition
τ	Shear pressure
∞	Freestream condition

Superscript

| T | Transpose |
| ˆ | Normalized quantity, $\hat{\bullet} = \frac{\bullet}{||\bullet||_2}$ |

I.   Introduction

A.   Motivation

SPACE situation awareness has come to the forefront of public cognizance with recent collisions between satellites and orbiting debris in near Earth orbits. With many crucial assets sharing near-Earth orbits with decommissioned satellites and other space debris, it is important to develop methods that can track these resident space objects (RSO) with high accuracy and over long periods of time to minimize probabilities of collision.[1]

Many objects in the Space Catalog receive significant perturbing forces due to Earth's atmosphere, which produces aerodynamic forces that act on these bodies. Currently, there are two approaches to fast modeling of aerodynamic forces: geometry simplification and time-averaging. In the case of the cylinder, for example, special cases have been solved analytically by fixing the freestream flow to the longitudinal or lateral axes. In reality, a cylindrical body will likely rotate and experience a range of freestream flows. Aerodynamics on a tumbling cylinder have previously been time-averaged across a cycle,[2] though these quantities are less preferable in state-space orbit propagation compared to the instantaneous quantities that analytic expressions can provide.

In order to develop analytic aerodynamic expressions for complex geometries, the previous research on primitive geometries must be expanded. This investigation provides validated models of the force and moment coefficients of such primitive shapes as the sphere, cylinder, panel, and rectangular prism. By generating analytic models for these primitive geometries without restricting the freestream direction, more complex geometries can be aerodynamically characterized.
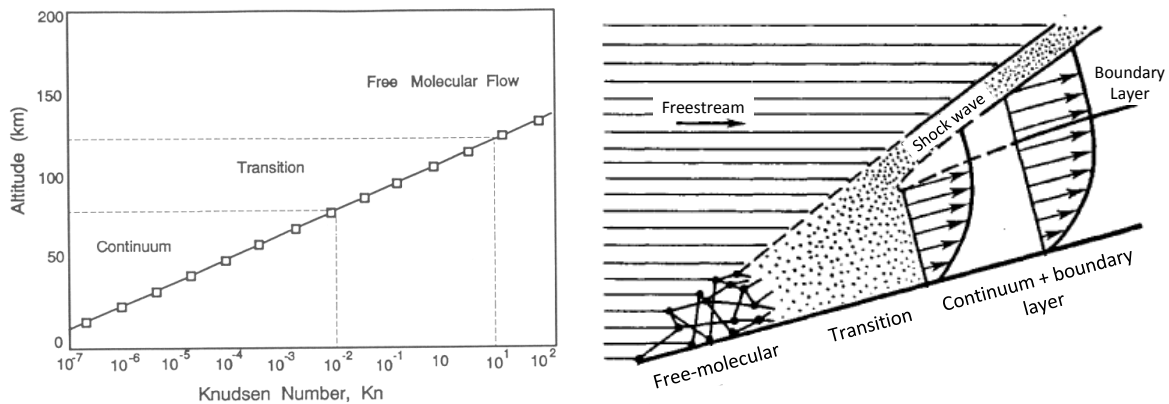
B.   Background

Aerodynamic forces and moments are used to catalog the momentum transfer from the flow surrounding a moving object. All fluid flow fields adhere to three conservation laws: mass, momentum, and energy.[3] When a molecule is introduced to a flow and it is immediately indistinguishable from the other molecules, the flow is considered to be a continuum and governed by the Navier-Stokes equations, a simplification of the

Boltzmann equation. Recently high-fidelity, analytical expressions for continuum hypersonic aerodynamics have been developed for a general range of shapes and these have enabled fast propagation of trajectories for various range of vehicles.[4,5,6] Although these methods have been originally developed for hypersonic, continuum flow, the general methodology can be extended to rarefied aerodynamics, especially free-molecular flow which is the regime of aerodynamics experienced by RSOs at the edge of Earth's atmosphere.

When the atmosphere is rarefied, the Boltzmann equation cannot be simplified to Navier-Stokes and molecular mechanics dominate the flow.[3] In rarefied flow, the interaction between molecules and their collisions with the surface of the object have to be accounted and this is accomplished by numerically solving the Boltzmann equation in a manner that is time intensive. Mean free path (λ), a dimensional quantity that depends on the number density (related to the mass density) of the local atmosphere, captures the distance a molecule can travel on average before some form of collision. The Knudsen Number (Kn), as shown in Eq. (1), is the characteristic value and is a representation of the distance between molecular collisions.

$$\mathrm{Kn} = \frac{\lambda}{l} \tag{1}$$

A high Knudsen Number is characteristic of rarefied flow, while low Knudsen number is characteristic of continuum flow. Figure 1(a) shows the expected Knudsen numbers and the flow type for a 1-m-long vehicle at different altitudes.[3] Based on the Knudsen number classification shown in the figure, the high altitude region where most RSO orbits reside is characterized by free-molecular flow.

(a) Knudsen number vs. altitude for a 1-m-long object.[3] (b) Flow behavior from free-molecular to continuum.[7]

Figure 1. Schematic of Free-molecular regime flow and its extent in atmosphere.

Free-molecular flow is a regime characterized by extreme rarefaction of the atmosphere. A molecule can travel long distances (relative to the characteristic length of the body) without collisions. Additionally, it can be assumed that the flow incident on the body is independent of any effect of the particles reemitted from the surface of the body after collision. Hence, the incident flow is entirely undisturbed by the presence of the body.[8] Figure 1(b) shows a schematic of flow in the free-molecular regime and also describes the transition from free-molecular to continuum flow. Although the figure is not to scale, it is descriptive of the free molecular flow and one can see that neither shock waves nor boundary layers have any effect on the flow incident on the body in free-molecule flow.[8]

C. Scope of the Work

This investigation builds on previous efforts[9,10,11] to derive analytic aerodynamic coefficients for primitive shapes in rarefied flow. The primitives in this paper, including panels, prisms, spheres, and cylinders have advantageous properties which simplify the process of developing the aerodynamic coefficients, such as a lack of concavity.

American Institute of Aeronautics and Astronautics

II. Methodology

A. Physical Model

Models for free-molecular flow build on energy and momentum transferred from the particles in the flow to an elemental surface area through the particle-surface interaction. The molecule-surface interaction is problem-dependent and is typically classified by one of two mechanisms: specular or diffuse. Specular reflection assumes that the molecular-surface interaction is elastic during which the tangential momentum is preserved and the normal momentum is reversed. Diffuse reflection assumes that the interaction is inelastic and the velocity of the reflected particle is based on a Maxwellian distribution dependent of the temperature of the reflected molecule and not the incident momentum.[3] Figure 2 shows a schematic of the two types of reflection mechanisms.
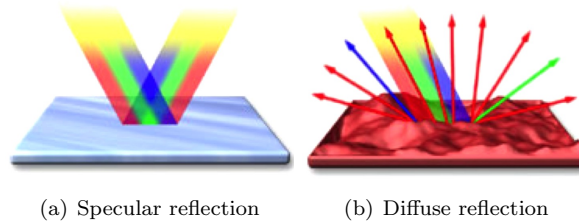

(a) Specular reflection   (b) Diffuse reflection

Figure 2. Models for molecular-surface interactions.[12]

The aerodynamic and heating properties due to the molecular-surface interaction is a function of the momentum and energy of the incident molecule, the reflected molecule, and the wall temperature. The incident molecule has properties based on freestream conditions, while the surface can be assumed to have a certain wall temperature. The properties of the reflected molecule, however, can be highly problem-dependent. The reflected molecule's properties are often characterized in terms of accommodation coefficients. The normal momentum accommodation coefficient (σ_N) describes the change in normal momentum due to the molecular-surface interaction, while the tangential momentum accommodation coefficient (σ_T) describes the momentum change in the tangential direction. These quantities are described in Eqs. (2) and (3).[8] Note that p is pressure (normal to the surface) and τ is the shear pressure and they designate conditions of the incident molecules (subscript i), the reflected molecules (subscript r), or the wall (subscript w). Represented values σ_N and σ_T can be found in found in Ref. 13. Specular reflection simplifies to $\sigma_N = \sigma_T = 0$, while diffuse reflection is $\sigma_N = \sigma_T = 1$.[3]

$$\sigma_N = \frac{p_i - p_r}{p_i - p_w} \tag{2}$$

$$\sigma_T = \frac{\tau_i - \tau_r}{\tau_i} \tag{3}$$

B. Analytic Aerodynamic Coefficients

Based on the above nomenclature, Schaaf and Chambre[8] theorized that the pressure coefficient (C_p) and the shear pressure (C_τ) coefficients on an elemental area inclined to the freestream at an angle θ can be described as shown in Eqs. (4) and (5), which was later presented in modified format by Regan and Anandakrishnan.[3] The freestream molecular speed ratio, s, is analogous to the Mach number and defined in Eq. (6), where V_∞ is the freestream velocity, R is the gas specific constant, and T_∞ is the freestream temperature. Similarly, T_w is the wall temperature. Eqs. (4) and (5) can be integrated over the surface of a general shape to provide the aerodynamic force and moment coefficients. It should be noted that unlike previous works regarding analytic hypersonic continuum aerodynamic coefficients by Grant,[4,5,6] the tangential momentum component cannot be ignored in the case of free-molecular flow aerodynamics.

American Institute of Aeronautics and Astronautics

$$C_p = \frac{1}{s^2} \left[\left(\frac{2 - \sigma_N}{\sqrt{\pi}} s \sin(\theta) + \frac{\sigma_N}{2} \sqrt{\frac{T_w}{T_\infty}} \right) e^{-(s \sin \theta)^2} \right. \tag{4}$$
$$\left. + \left\{ (2 - \sigma_N) \left((s \sin \theta)^2 + \frac{1}{2} \right) + \frac{\sigma_N}{2} \sqrt{\frac{\pi T_w}{T}} s \sin \theta \right\} (1 + \text{erf}(s \sin \theta)) \right]$$

$$C_\tau = -\frac{-\sigma_T \cos \theta}{s \sqrt{\pi}} \left[e^{-(s \sin \theta)^2} + \sqrt{\pi} s \sin \theta \left(1 + \text{erf}(s \sin \theta) \right) \right] \tag{5}$$

$$s = \frac{V_\infty}{\sqrt{2 R T_\infty}} \tag{6}$$

In the free molecular regime, the mean free path of the gas is many times larger than the characteristic dimension of the body. The gas flow is assumed to be of an infinite extent, which is valid for high altitude considerations. A consequential assumption of the extreme rarefaction is that the indent flow is entirely undisturbed by the presence of the body and, at the body, the approaching gas is assumed to be in Maxwellian equilibrium. The formulation for the pressure and shear coefficients in Schaaf and Chambre utilize two accommodation coefficients, σ_N and σ_T, which are averaged quantities, so the models presented in Eqs. 4 and 5 are valid so long as these coefficients adequately accommodate the incident and reflected energies. Specifically, the accommodation coefficients are valid in gases which have significantly less vibrational energy compared to translational and rotational energy.

The challenge of finding analytical aerodynamics is integrating the pressure coefficient (Eq.(4)) and shear pressure coefficient (Eq.(5)) expressions over the surface of a body. The elemental force ($\mathbf{df}$) applied over an differential area (dA) consists of pressure and shear pressure components, with the pressure working along the normal vector ($\hat{\mathbf{n}}$) and the shear pressure working along the tangential vector ($\hat{\mathbf{t}}$) as seen in Eq. (7). Note that the normal vector is defined as positive outwards. Additionally, using conventional flight dynamics body axes,[14] the normalized velocity vector ($\hat{\mathbf{V}}_\infty$) can be defined in terms of the angle of attack (α) and the sideslip angle (β) as shown in Eq. (8). Then the force and moment coefficients in the x, y, and z body directions can be found by surface integration as shown in Eqs. (9) and (10). The force coefficients consist of axial (subscript A), side (subscript S), and normal (subscript N) forces and the moment coefficients consist of rolling (subscript l), pitching (subscript m), and yawing (subscript n) moment coefficients. The position vector of the element ($\mathbf{r}$) is defined from the origin of the coordinate system about which the forces and moments are taken - in this case the body frame of the vehicle.

$$\mathbf{df} = \left(C_p \hat{\mathbf{n}} + C_\tau \hat{\mathbf{t}} \right) dA \tag{7}$$

$$\hat{\mathbf{V}}_\infty = - \left[\cos \alpha \cos \beta \quad \sin \beta \quad \sin \alpha \cos \beta \right]^T \tag{8}$$

$$\begin{bmatrix} C_A \\ C_S \\ C_N \end{bmatrix} = \frac{1}{A_{\text{ref}}} \iint_S \mathbf{df} \tag{9}$$

$$\begin{bmatrix} C_l \\ C_m \\ C_n \end{bmatrix} = \frac{1}{A_{\text{ref}} \cdot l_{\text{ref}}} \iint_S \mathbf{r} \times \mathbf{df} \tag{10}$$

C.   Parameterization Schema

The integrals in Eqs. (9) and (10) are performed over the surface of the body, which must be parametrized in a fashion to give the position vector of every point on the surface. The position vector for this method must be parametrized by two independent variables u and v. Additionally, due to the convention used in this method, u and v must be chosen such that $\mathbf{r}_u \times \mathbf{r}_v$ is the non-normalized normal vector pointed outwards from the surface, where $\mathbf{r}_u = \frac{\partial \mathbf{r}}{\partial u}$ and $\mathbf{r}_v = \frac{\partial \mathbf{r}}{\partial v}$. Similarly, the differential area, dA, can be shown to be $dA = \|\mathbf{r}_u \times \mathbf{r}_v\|_2$.

The outward unit normal vector is the cross-product of the partial of the position vector with respect to u and the partial of the position vector with respect to v as shown in Eq. (11). Equation (12) shows that the unit normal vector and the unit velocity vector can be used to define the local flow angle θ that appears

American Institute of Aeronautics and Astronautics

in the pressure and shear pressure coefficient expressions. The definition of the local flow angle also helps resolve the definition of the unit tangential vector, $\hat{\mathbf{t}}$, that defines the direction in which the shear pressure coefficient is acting. Unlike the normal vector, there are infinite choices for the tangential vector in the plane tangent to the elemental surface. For example, either $\mathbf{r}_u$ or $\mathbf{r}_v$ is an acceptable choice for a tangential vector. But based on definition of the shear pressure, which is based on the shear force, the proper vector is opposite of the local flow direction. This is described by Eq. (13). These quantities and the relationships between them are illustrated in Figure 3.

$$\hat{\mathbf{n}} = \frac{\mathbf{r}_u \times \mathbf{r}_v}{||\mathbf{r}_u \times \mathbf{r}_v||_2} \tag{11}$$

$$\sin\theta = -\hat{\mathbf{V}}_\infty \cdot \hat{\mathbf{n}} \tag{12}$$

$$\hat{\mathbf{t}} = \frac{\hat{\mathbf{n}}\left(\hat{\mathbf{V}}_\infty \cdot \hat{\mathbf{n}}\right) - \hat{\mathbf{V}}_\infty}{\sqrt{1 - \left(\hat{\mathbf{V}}_\infty \cdot \hat{\mathbf{n}}\right)^2}} \tag{13}$$

A variety of shapes are analyzed in this paper for their aerodynamic coefficients, and while there are many methods to parameterize a surface, the following methods have yielded integrable analytic aerodynamic coefficients for rarefied flow.
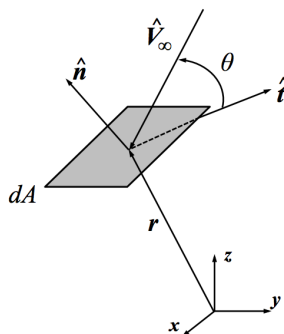

Figure 3. Vector diagram illustrating the relationships between relevant quantities.

1. Triangular Panel

A triangular panel can be created from three position vectors, $\triangle ABC = (\mathbf{r}_A, \mathbf{r}_B, \mathbf{r}_C)$, to the vertices where A, B, and C are defined counterclockwise about the origin. From these three vectors, two can be defined as $\mathbf{r}_1 = \mathbf{r}_B - \mathbf{r}_A$ and $\mathbf{r}_2 = \mathbf{r}_C - \mathbf{r}_A$, which are in the plane of the panel. The parameterization of the triangular panel is given by Eq. (14). A visual of the parameterization of the triangular panel is given in Figure 4. Though the parameterization given below describes a triangle, the aerodynamic coefficients for the panel are not dependent on the geometry of the panel.

$$\mathbf{r} = u\,\mathbf{r}_1 + v\,\mathbf{r}_2 \tag{14}$$

The limits on u and v in the (u,v)-plane are the positive axes and the line $u + v = 1$. By defining the vectors to the vertices of the triangle in a counterclockwise sense, the normal vector is guaranteed positive.

2. Rectangular Panel

A rectangular panel can be defined by the vector to the center of the rectangle and two vectors to the long and short sides of the triangle. Let $\mathbf{r_c}$ be the vector to the center and $\mathbf{a}$ and $\mathbf{b}$ be the vectors to each side of rectangle. The vectors should satisfy the triple product inequality $(\mathbf{a} \times \mathbf{b}) \cdot \mathbf{r_c} \leq 0$ so that the normal vector is outward facing. The square panel can be parameterized in the same way, with the condition that $||\mathbf{a}||_2 = ||\mathbf{b}||_2$. The parameterization of the rectangular panel is given by Eq. (15) and u and v are independently bounded on the interval $[-1, 1]$. The rectangular panel parameterization is illustrated
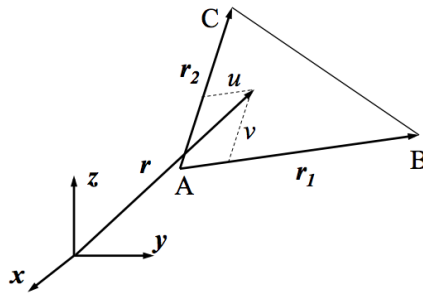
American Institute of Aeronautics and Astronautics

Figure 4. Illustration of the surface parameterization of the triangular panel.

in Figure 5. The rectangular prism is the composition of six rectangular panels and the aerodynamics of each panel are combined by the method described in Section F.

$$\mathbf{r} = \mathbf{r_c} + u\,\mathbf{a} + v\,\mathbf{b} \tag{15}$$
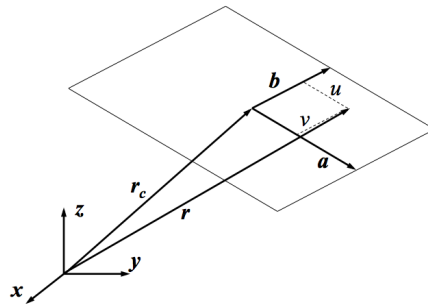

Figure 5. Illustration of the surface parameterization of the rectangular panel.

3. Sphere

The sphere is is defined as the collection of points in 3-dimensional space that are equidistant from a center. In this case, the center of the sphere is assumed to be the center of the reference frame. Since drag is the only aerodynamic force on the sphere, a solution for the drag on the sphere can be calculated in the wind frame and then rotated through α and β to find the body-axis coefficients. In this case, the sphere has a single parameter, the radius (R), and is defined in spherical coordinates as shown in Eq. (16). The bounds on the parameters u and v are $[0, \pi]$ and $[0, 2\pi]$, respectively. Figure 6 illustrates this parameterization scheme.

$$\mathbf{r} = R\left[\sin u \cos v \quad \sin u \sin v \quad \cos u\right]^{T} \tag{16}$$
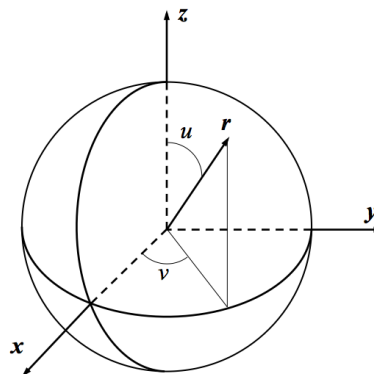

Figure 6. Illustration of the surface parameterization of the sphere.

American Institute of Aeronautics and Astronautics

4. Cylinder

The cylinder is a rectangle of revolution and is characterized by its radius (R) and length (l). Let the axis of the cylinder coincide with the first axis of the reference frame and the center of the frame be located at half the length, then the cylindrical hull can be parameterized by Eq. (17), where u is bounded by $[0, 2\pi]$ and v is bounded by $[-l/2, l/2]$. This surface parameterization is illustrated in Figure 7.

$$\mathbf{r} = \begin{bmatrix} v & R\cos u & R\sin u \end{bmatrix}^T \tag{17}$$
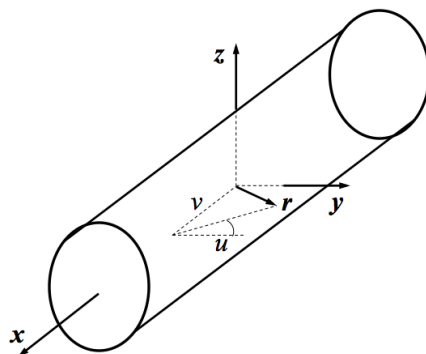

Figure 7. Illustration of the surface parameterization of the cylinder.

The ends of the cylinder are circles parameterized by Eq. (18) with u bounded by $[0, R]$ and v bounded by $[0, 2\pi]$. The sign of the first component of the position vector is equal to the sign of the outward normal vector of the circle.

$$\mathbf{r} = \begin{bmatrix} \pm\dfrac{l}{2} & u\cos v & u\sin v \end{bmatrix}^T \tag{18}$$

D.   Concavity Constraint

Each of the above geometries satisfies the conditions of convex functions, $\partial_u^2 \mathbf{r} \leq 0, \partial_v^2 \mathbf{r} \leq 0, \partial_{uv}^2 \mathbf{r} \leq 0$, thereby simplifying the process of defining the wetted area of the object. On a non-concave object, there are always two distinct regions of the surface, the wetted region and the shadowed region. The boundary between these regions occurs when the sine of the local freestream angle transitions from positive to negative. For a non-concave shape, this condition is equivalent to $\sin\theta = 0$. Using a single condition to describe the boundary of the wetted region reduces the complexity of solving the integrals of elemental forces by simplifying the bounds of integration.

E.   Surface Parameterization Bounds

On convex geometries, the surface is separated into two disjoint regions where the interface between these regions occurs when the freestream velocity is orthogonal to the local normal direction. Choosing which region is the wetted region can be found by calculating the local angle at a single point, however in all cases in this paper *a priori* knowledge of the geometry distinguished the wetted area from the shadowed area. The parameterizations of the objects listed above are not unique, there are an infinite number of parameterization schema for a single geometry, however they were selected for simplicity in the limits of integration for the wetted area. For example, the sphere could be parameterized by $\mathbf{r} = \begin{bmatrix} \sqrt{R^2 - (y^2 + z^2)} & y & z \end{bmatrix}^T$, however the bounds on the inner integral become circular segments. In the (y, z)-plane the region of integration is a circle, whereas in the (u, v)-plane the region of integration is a rectangle, which reduces the computational effort to evaluate the integrals. Each of the above geometries are bounded in their (u, v)-planes by a rectangle, except the triangular panel which is bounded by a right triangle.

The wetted regions of these geometries are not as simple as a rectangle or a triangle. Though the area of the wetted region is dependent on the direction of the freestream velocity, the shape of the region is consistent. For example, the wetted area of the cylinder and the sphere are rectangular subregions.

American Institute of Aeronautics and Astronautics

F. Application of the Heaviside Step Function

Some geometries are piecewise parameterized, such as the rectangular prism where each of the faces is individually parameterized. Since each panel's contribution to the overall force and moment coefficients depends on whether it is wetted by the flow, a novel approach used in this work is to introduce the Heaviside step function. The Heaviside function behaves like a switch toggling the force and moment coefficients of each panel. The prism and the cylinder are both piecewise parameterized, and the general form for the application of the Heaviside function is shown in Eq. (19).

$$
\begin{bmatrix} C_A \\ C_S \\ C_N \end{bmatrix} = \sum_i \begin{bmatrix} C_A \\ C_S \\ C_N \end{bmatrix}_i H\left(-\hat{\mathbf{V}}_\infty \cdot \hat{\mathbf{n}}_i\right)
\tag{19}
$$

The same approach is used for the force and moment coefficients. The argument of the Heaviside function is equivalent to the sine of the local flow angle. For all negative inputs to the Heaviside function, the output is a zero, so the shadowed panels make no contribution to the overall force and moment coefficients. Likewise, the panels that are wetted by the flow have a positive sine of the local flow angle and their force and moment coefficients contribute to the overall coefficients. The summation of these contributions is a result of the linearity of the integral operator.

Although panel methods have been developed in the past, the description of the various panels is included in this paper because it is a primary component of the method used to analyze the rectangular prism and the cylinder. The approach to solving for the aerodynamics in this investigation is novel in its application of the Heaviside step function to closed piecewise parameterized surfaces. The method described below is applicable beyond the shapes described so long as the shape is closed, piecewise, and convex.

III. Results

A. Validation Method

The aerodynamic analytical expressions derived by the method above are validated against industry-standard free-molecular aerodynamics prediction tools like Direct Simulation Monte Carlo (DSMC) codes. DSMC codes solve the Boltzmann equations directly, but are computationally expensive. However, they serve as a good way to check the accuracy of the analytical expressions. The specific DSMC code used here for comparison is the NASA-developed DSMC Analysis Code (DAC) that has been tested and used in the field extensively.[15, 16, 17] The version of the code used in the analysis is DAC97-N from October 2012.

DSMC tools like DAC have several types of input files and parameters that have to be adjusted in order to achieve realistic aerodynamic predictions. On the other hand, the analytical expressions developed from the C_p and C_τ expressions in Eqs. (4)- (5) are only a function of the molecular speed ratio, wall temperature, freestream temperature, and the dynamics of the interaction that is captured by the normal and tangential momentum accommodation coefficients. Hence, one can easily see some of the advantages in complexity offered by analytical aerodynamic expressions.

B. Convex Geometries

1. Sphere

Analytical expressions for the drag coefficient (C_D) of a sphere were developed using the methodology above. These expressions are not novel, since Schaaf and Chambre[8] also developed similar expressions for free-molecular flow over a sphere. But this problem is a very simple first step to test the accuracy of the analytical prediction methodology, since all aerodynamic force and moment coefficients are zero except for the drag force for flow over a sphere with the center of pressure at the center of gravity of the sphere. Expressions for the force coefficients, moment coefficients, and stability derivatives of the sphere can be found in this file embedded in the paper (analyticExpressions.nb) and are presented in a *Mathematica* notebook[a].

Comparisons between DAC results (colored dots) and the analytical expression (lines) are given in Fig. 8. Diatomic nitrogen was used as the freestream gas in the simulation. Variation of the drag force coefficient over a range of atmospheric speeds (related to the molecular speed ratio), wall temperatures, and freestream

---

[a]For best results use Adobe Acrobat readers The embedded file can be downloaded from the link.

temperatures are shown in the figure to illustrate the range of conditions for which the analytic model is valid. Note that the pure specular and pure diffuse bounds are shown. Aerodynamic parameter values for conditions other than these two extremes will fall in the shaded zone. The baseline flow parameters are $T_w = 300K$, $T_\infty = 973K$, and $V_\infty = 7500$ m/s, and each graph shows the effect of shifting these values. The specular and diffuse flow relations are shown for each of the three sensitivity cases.
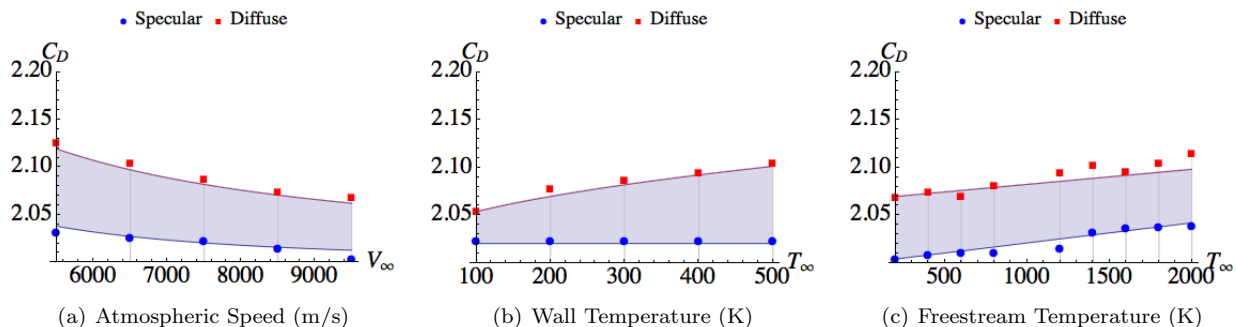

| (a) Atmospheric Speed (m/s) | (b) Wall Temperature (K) | (c) Freestream Temperature (K) |

Figure 8. Validation of analytical expressions for sphere in free-molecular flow.

Figure. 8 shows that the analytical expressions and the DAC predictions match very well. The slight discrepancies between the two can be attributed to adjustments that need to be made to the DAC computation grid. In the case of the sphere, drag is the only force acting on the body, so the aerodynamic force is resolved into the wind frame. All proceeding geometries resolve the aerodynamic forces and moments into the vehicle body axes.

2. Cylinder

The analytic force and moment coefficients on the cylinder were derived by taking advantage of the axial symmetry of the body. This means that the freestream can be restricted to the body's (x, y)-plane, effectively collapsing the angle of attack (α) to zero and letting the side slip angle (β) vary on the interval $[0, \pi/2]$. Every freestream orientation can be x-rotated to lie in the first quadrant of the (x, y)-plane, so these results can be x-rotated to any other freestream orientation. The analytic results of this equation, for the same conditions as in Section B.1 above and a length-to-diameter ratio of 2.18, with the side slip angle varied on the range $[0, \pi/2]$, are compared to DAC numerical simulation data in Figure 9. The two cases of specular and diffuse reflections are plotted together to illustrate the range of valid solutions which the analytical model can be applied.

The specular results show the best agreement between DAC and the analytic model, although there is still good agreement between the two types of analysis for the diffuse results. The results of the two analyses differ in cases where there is a small angle between the freestream and the circular face of the cylinder. This effect is apparent in each of the above plots, and most noticeable in Figure 9(f). A small local freestream angle corresponds to significant tangential forces, which explains the "tails" on the yawing moment graph. The effect is also evident on the diffuse curves in the force coefficient graphs.

The tails on the graphs of the yawing moment in the cylinder and the prism under diffuse reflections are indicative of a discrepancy between the analytic model and DAC. The DAC data tend to show very little variation on the moment coefficients on these geometries, though these coefficients vary significantly with the direction of the freestream velocity. For the case of the rectangular prism, which is covered in Sec. C. 2, the moment coefficients are zero when the freestream flows along one of the body axes, which is shown in the DAC data. If the freestream velocity's orientation is perturbed even by a small margin, there is significant tangential forces on the exposed surfaces, causing the object to rotate. The object will continue to rotate until the moments due to the tangential forces are balanced, which indicates that the moment coefficient ought to change with respect to the orientation of the freestream. The analytic models feature this change in the moment coefficients, while the DAC results do not. Future investigation will determine why the DAC data does not show such behavior for diffuse reflections.
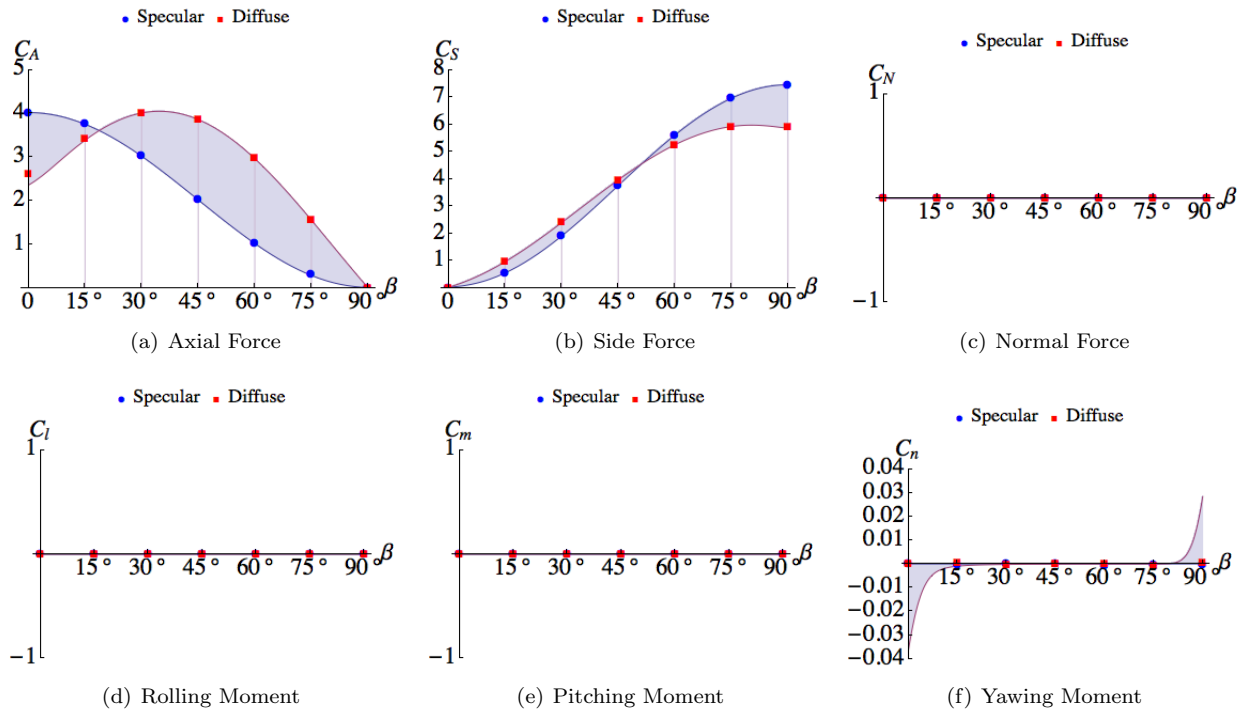
American Institute of Aeronautics and Astronautics

(a) Axial Force

(b) Side Force

(c) Normal Force

(d) Rolling Moment

(e) Pitching Moment

(f) Yawing Moment

Figure 9. Validation of the aerodynamic coefficients of the cylinder.

C. Planar Geometries

1. Panel

Although a simple shape, a panel is considered in this study since it is a fundamental geometry and the primary shape of stereolithography files, which can be produced by most Computer-aided design (CAD) software. The analytic results of this equation are for the same conditions as those introduced in Section B.1, with the angle of attack (α) and side slip angle (β) independently varied on the range $[0, 2\pi]$. The analytical results are once again compared with DAC numerical simulation data. In Fig. 10, the force coefficients of the panel are illustrated with the angle of attack fixed.
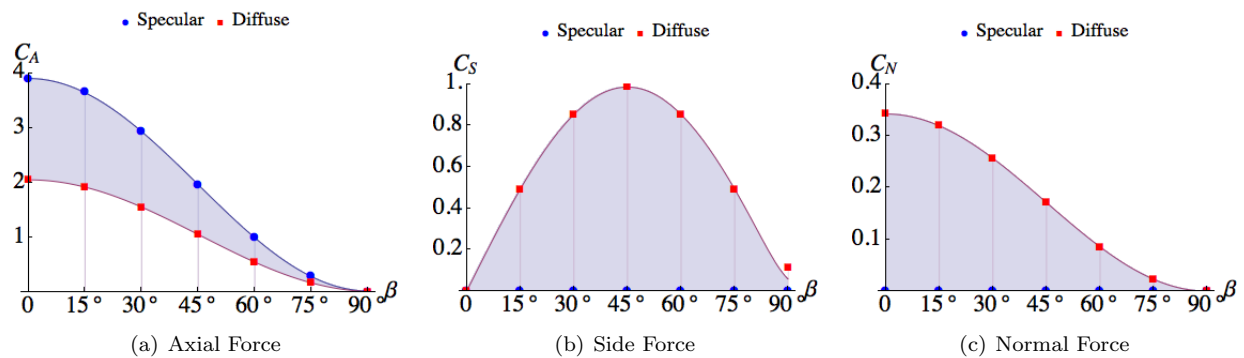

(a) Axial Force

(b) Side Force

(c) Normal Force

Figure 10. Validation of the aerodynamic coefficients of the panel.

2. Rectangular Prism

The analytic force and moment coefficients on the cylinder were derived by taking advantage of the piecewise composition of the geometry. By applying the Heaviside function to toggle a panel's contribution depending on if it is wetted by the flow or not, the force and moment coefficients are calculated by the sum of the contributions from all panels. The analytic results of this equation, for the same conditions as in Section

American Institute of Aeronautics and Astronautics

B.1, are compared with the DAC data. Graphs of the coefficients in the case of $T_w = 300K$, $T_\infty = 1100K$, and $V_\infty = 7500$ m/s, equal side lengths, and $\alpha = 10°$ are given in Figure 11.

(a) Axial Force   (b) Side Force   (c) Normal Force

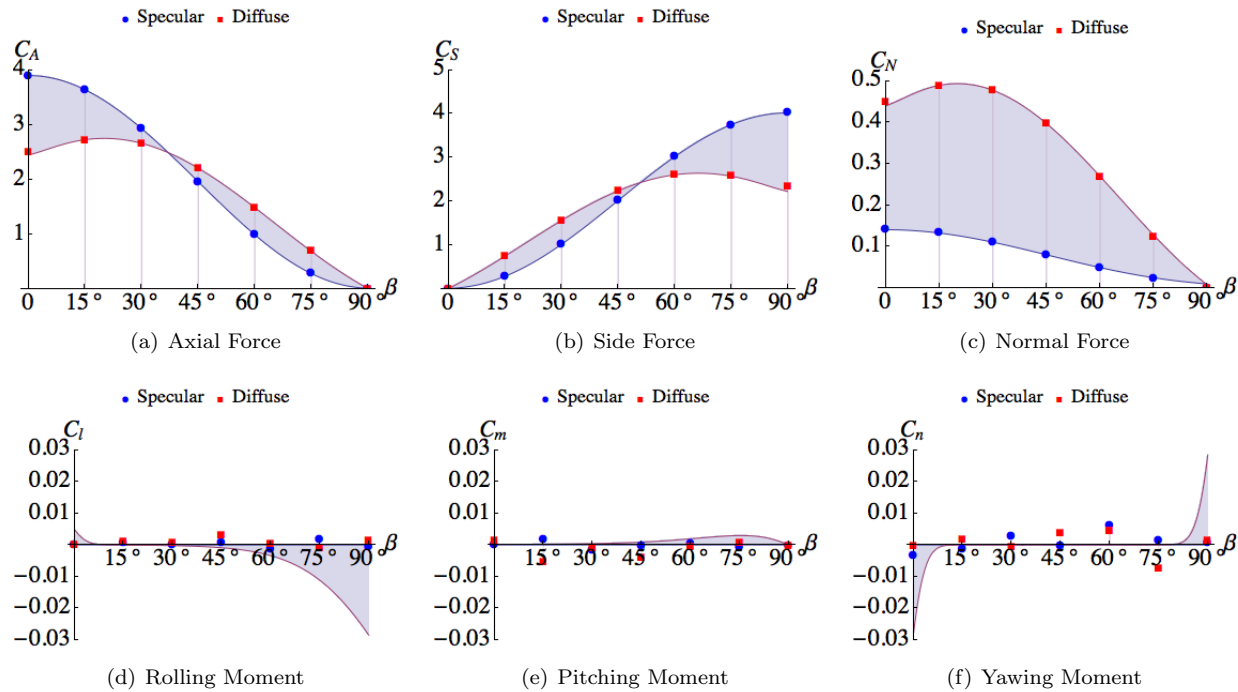(d) Rolling Moment   (e) Pitching Moment   (f) Yawing Moment

Figure 11. Validation of the aerodynamic coefficients of the rectangular prism.

D. Analysis

1. Model Accuracy

The equations for the pressure and shear coefficients given in Eqs. (4)- (5) are models of rarefied flow and are not derived from the governing equation for the flow. To quantify the goodness-of-fit for these models, the R^2 values for the force and moment coefficients are tabulated relative to the DAC results in Table 1. The median percent error is given in Table 2 as an additional metric for the accuracy of the analytic models. In cases where the theoretical aerodynamic coefficient is zero, the statistical fit values are not provided. The diffuse moment coefficients for the cylinder and the prism are not included in the model accuracy analysis due to the still unresolved reason disagreement between the analytic model and DAC.

Table 1. R^2 values for DAC results relative to the analytic model.

Geometry	Specular						Diffuse					
	C_A	C_S	C_N	C_l	C_m	C_n	C_A	C_S	C_N	C_l	C_m	C_n
Sphere	0.667	-	-	-	-	-	0.813	-	-	-	-	-
Cylinder	0.999	0.999	-	-	-	-	0.994	0.999	-	-	-	-
Panel	0.999	-	-	-	-	-	0.999	0.996	0.999	-	-	-
Rectangular Prism	0.999	0.999	0.994	-	-	-	0.999	0.997	0.999	-	-	-

2. Computational Comparison

The large compute time for aerodynamic coefficients is usually a major hindrance for rapid exploration of designs of rarefied flow vehicles or predicting the trajectories of resident space objects with high accuracy. The advantages of analytical expression can be easily seen in Table 3 that lists the run times for the analytical expressions for various shapes. For reference, the analytical computations were tested on a 2.8 GHz Intel

American Institute of Aeronautics and Astronautics

Table 2. Median absolute percent errors for DAC results compared to the analytic model.

Geometry	Specular						Diffuse					
	C_A	C_S	C_N	C_l	C_m	C_n	C_A	C_S	C_N	C_l	C_m	C_n
Sphere	0.137	-	-	-	-	-	0.380	-	-	-	-	-
Cylinder	0.085	0.069	-	-	-	-	0.262	0.265	-	-	-	-
Panel	0.153	-	-	-	-	-	0.078	0.140	0.231	-	-	-
Rectangular Prism	0.260	0.089	0.711	-	-	-	0.213	0.352	0.322	-	-	-

Core 2 Duo processor. In general, the DAC run times vary based on the resolution of the model, but for comparison DAC needed 16 minutes on a 2.2 GHz duo-core processor to analyze the simple sphere. The analytic expression for drag on a sphere ran 870,000 times faster than DAC.

Table 3. Mean run time comparison of analytic and numerical methods for determining aerodynamic coefficients.

Geometry	Analytic Runtime (ms)
Sphere	1.1
Cylinder	22
Panel	2.4
Rectangular Prism	23

IV. Conclusions

Fields such as space situational awareness could benefit significantly from fast and accurate predictions of aerodynamic force and moment coefficients of objects in near-Earth orbits. The flow in near-Earth orbits is typically described as free-molecular flow and current methods of predicting aerodynamic coefficients in this regime require very computationally intensive methods that cannot be used in conjunction with fast trajectory propagations tools required for space situational awareness.

However, recent advances in symbolic manipulation software allows one to develop analytical expressions for aerodynamic quantities without making significant assumptions or simplifications. This analytical aerodynamic expression method has been used for hypersonic, continuum flow in the past and the current work advances this method for free-molecular flow. These expressions are validated against state-of-the-art engineering tools, specifically DAC. The results of the analytical method and the numerical tool agreed very well for force coefficient expressions for spheres, cylinders, triangular panels, and rectangular prisms and had good agreement over large orientation angle ranges for the moment coefficients. This initial study of analytically derived rarefied flow aerodynamic coefficients shows promise and future work will include derivation of analytic expressions for a larger range of primitive shapes, the composition of primitive geometries, and expressions for concave and arbitrary axisymmetric geometries.

Acknowledgments

References

[1]Bar-Shalom, Y., Li, X., and Kirubarajan, T., *Estimation with Applications to Tracking and Navigation*, John Wiley & Sons, Inc., New York, NY, 2001.

[2]Pilinski, M. D., Argrow, B. M., Palo, S. E., and Bowman, B. R., "Semi-Empirical Satellite Accommodation Model for Spherical and Randomly Tumbling Objects," *Journal of Spacecraft and Rockets*, Vol. 50, No. 3, July 2013, pp. 556–571.

[3]Regan, F. J. and Anandakrishnan, S. M., *Dynamics of Atmospheric Re-Entry*, American Institute of Aeronautics and Astronautics, Reston, VA, 1993.

[4]Grant, M. J. and Braun, R., "Analytic Hypersonic Aerodynamics for Conceptual Design of Entry Vehicles," AIAA 2010-1212, *48th AIAA Aerospace Sciences Meeting,* Orlando, FL, 2010.

[5]Grant, M. J. and Braun, R., "The Extension of Analytic Hypersonic Force Coefficients for Conceptual Design Using the Divergence Theorem," AIAA 2012-4580, *AIAA Atmospheric Flight Mechanics Conference,* Minneapolis, MN, 2012.

[6]Grant, M. J., "The Construction of Analytic Hypersonic Pitch Moment Coefficients Using a Curl Transformation," AIAA 2013-0225, *51st AIAA Aerospace Sciences Meeting,* Dallas, TX, 2013.

[7]Vallander, S. V., "Collection 1," *Aerodinamika Razrezhennykh Gazov*, 1963.

[8]Schaaf, S. A. and Chambre, P. L., *Flow of Rarefied Gases*, Princeton University Press, 1961.

[9]Wang, C.-T., "Free Molecular Flow over a Rotating Sphere," *AIAA Journal*, Vol. 10, 1972, pp. 713–714.

[10]Yoshizawa, Y., "Examination of the Usefulness of the Restricted Hermite Expansion Method for Rarified Gas Dynamics Problems," *Progress in Astronautics and Aeronautics*, Vol. 74, 1980, pp. 371–385.

[11]Stalder, J. and Zurick, V., "Theoretical Aerodynamic Characteristics of Bodies in a Free-Molecule-Flow Field," Tech. rep., NACA TN 2423, 1951.

[12]Davidson, M. W., "Specular and Diffuse Reflection," Electronic, June 2006.

[13]Hurlbut, F. C., *Encyclopedia of Applied Physics*, chap. Rarefied-Gas Dynamics, Wiley-VCH Verlag GmbH & Co KGaA, 2003, pp. 97–115.

[14]Etkin, B., *Dynamics of Atmospheric Flight*, Dover Publications, Meneola, NY, 2000.

[15]LeBeau, G. and Lumpkin III, F., "Application highlights of the DSMC Analysis Code (DAC) software for simulating rarefied flows," *Computer Methods in Applied Mechanics and Engineering*, Vol. 191, 2001, pp. 595–609.

[16]Boyles, K., LeBeau, G., Lumpkin III, F., and Blanchard, R., "The Use of Virtual Sub-Cells in DSMC Analysis of Orbiter Aerodynamics at High Altitude Upon Reentry," AIAA 2003-1030, *41st Aerospace Sciences Meeting,* Reno, NV, 2003.

[17]LeBeau, G., "A User Guide For the DSMC Analysis Code (DAC) Software," Tech. Rep. DAC97-N, NASA JSC, 2012.